iScience

CellPress
OPEN ACCESS

Article

Perm-selective ultrathin high flux microporous polyaryl nanofilm for molecular separation

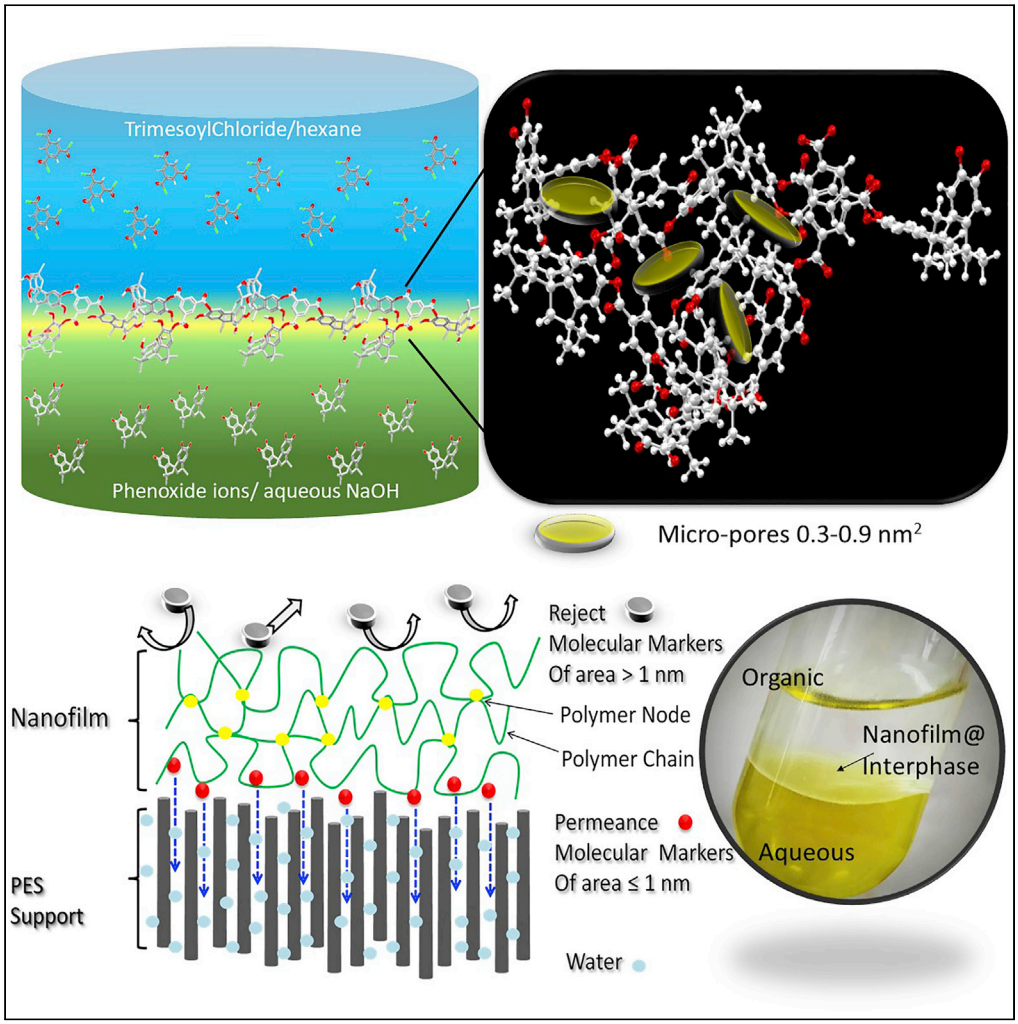

Ashwini Kaushik, Mansoor Dhundhiyawala, Priyanka Dobariya, Karan Marvaniya, Shilpi Kushwaha, Ketan Patel

shilpik@csmcri.res.in (S.K.)
ketanpatel@csmcri.res.in (K.P.)

Highlights

Ultrathin PAR composite membrane with crumpled morphology & improved permeance

Tailored surface functionality to improve hydrophilicity, negative surface charge

PAR membranes shows the high flux separation within 450 g/mol range of MWCO

Kaushik et al., iScience 25, 104441
June 17, 2022
https://doi.org/10.1016/j.isci.2022.104441

iScience

CellPress
OPEN ACCESS

Article

Perm-selective ultrathin high flux microporous polyaryl nanofilm for molecular separation

Ashwini Kaushik,[1,3] Mansoor Dhundhiyawala,[1] Priyanka Dobariya,[1,3] Karan Marvaniya,[2,3] Shilpi Kushwaha,[2,3,*] and Ketan Patel[1,3,4,5,*]

SUMMARY

Polymeric membranes with high permeance and selectivity performances are anticipated approach for water treatment. Separation membranes with moderate molecular weight cut-offs (MW in between 400 and 700 g mol^{-1}) are desirable to separate multivalent ions and small molecules from a water stream. This requires polymeric membranes with controlled pore, pore size distribution, surface charge, and thin active layer to maximize membrane performance. Here, a fabrication of the polyaryl nanofilm with thickness down to ~15 nm synthesized using interfacial polymerization onto ultrafiltration supports is described. Electron microscopy analysis reveals the presence of crumpled surface morphology in polyaryl nanofilm. Polyaryl nanofilm shows high water permeance of ~110 $Lm^{-2}h^{-1}$ bar^{-1}. Polyaryl nanofilm presents molecular weight cut-off greater than ~450 $gmol^{-1}$ (molecular marker) with water permeance of ~84 $Lm^{-2}h^{-1}$ bar^{-1}. Multivalent salt ($K_3[Fe(CN)_6]$) has higher rejection (>95%) as compared to the monovalent (~5%) and divalent salt (~28%) with the water permeance of ~81 $Lm^{-2}h^{-1}$ bar^{-1}.

INTRODUCTION

One of the landmark discovery in the processing of large-scale unit operation is separation and purifications of liquids and gases (Sholl and Lively, 2016). In this regime, membrane-based separation processes emerged as a gray research area owing to its cost effectiveness, low energy consumption, reduced operation time, low carbon footprints, continuous operation, and modular design as compared to other purifications processes such as distillation, evaporation, or adsorption (Werber et al., 2016). Successful examples of membrane-based technology are sea-water desalination using reverse osmosis (RO) membranes and water purifications using nanofiltration (NF). This membrane-based technology played a key role in providing safe fresh water, and thus emerged as a key process in reducing the shortage of fresh water.

Both RO and NF membranes made up of a thin separating layer on porous ultrafiltration support (Werber et al., 2016; Elimelech and Phillip, 2011). This separating layer is prepared by interfacial polycondensation (Termed as "Interfacial polymerization" (IP)) (Zhang et al., 2020), where polymerization reaction occurs in between the two immiscible phases, resulted in the polymer confined to the interface to form thin film of polymer (separation layer), as shown in Figure 1. The key function of the thin film is to provide solute selectivity and permeability, and these two major parameters primarily depends on the porosity, pore size distribution, thickness, and the surface charge (Werber et al., 2016; Elimelech and Phillip, 2011). Nanofiltration (NF) is a pressure driven membrane-based process, and it has been viewed as the key candidate for the treatment of wastewater to produce pure drinking water. Usually, it operates at low pressure and produces water with high water permeability ($\lesssim$10 L m^{-2} $hour^{-1}$ bar^{-1} ($Lm^{-2}h^{-1}bar^{-1}$) and exclude multivalent salts and organic molecules beyond 200 molecular weight (Fane et al., 2015). The major challenge in NF membrane is to overcome the trade-off between permeance and selectivity.

Last two decades have witnessed the architype swing to improve the separation performance of NF membranes in order to enhance the water permeability without changing the solute selectivity (Werber et al., 2016; Elimelech and Phillip, 2011; Geise et al., 2011; Rezakazemi et al., 2018). Few effective strategies

[1]Membrane Science and Separation Technology Division, CSIR Central Salt and Marine Chemicals Research Institute, Bhavnagar 364002, India

[2]Analytical and Environmental Science Division and Centralized Instrument Facility, CSIR Central Salt and Marine Chemicals Research Institute, Bhavnagar 364002, India

[3]Academy of Scientific and Innovative Research (AcSIR), Ghaziabad, Uttar Pradesh 201002, India

[4]Senior author

[5]Lead contact

*Correspondence: shilpik@csmcri.res.in (S.K.), ketanpatel@csmcri.res.in (K.P.)

https://doi.org/10.1016/j.isci.2022.104441

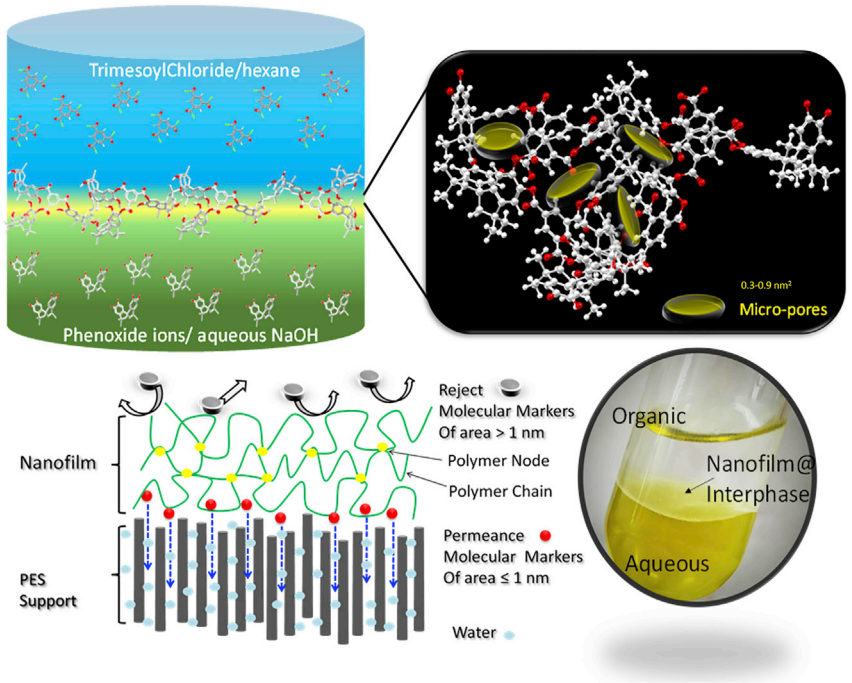

Figure 1. Scheme presence the formation of polyaryl nanofilm at the interphase and separation principle

used to enhance the water permeability include: (i) reducing the thickness of thin separating layer (Sarkar et al., 2020a, 2020b, 2021; Karan et al., 2015; Jiang et al., 2018), (ii) increasing the hydrophilicity of membrane surface (Zhang et al., 2018), (iii) tailoring the membrane surface structure (Zhang et al., 2018; Tan et al., 2018; Zhai et al., 2018), and (iv) increasing the free volume and developing interconnected voids inside membrane surface (Liang et al., 2018; Guiver and Lee, 2013; McKeown and Budd, 2006). Among all, fourth strategy attracted most of the exploration, mainly focused on incorporation of additives in the thin separating layer and creating free volume in polymer thin film. Several types of nanofillers exploited for the purpose, i.e. zeolite (Liu et al., 2015), titanium dioxide (Soroko and Livingston, 2009; Cheng et al., 2017), cerium dioxide nanoparticle (Tavangar et al., 2020), graphene oxide (Hu et al., 2017; Sarkar et al., 2020a, 2020b), carbon nanotubes (Shen et al., 2013; Sarkar et al., 2020a, 2020b; Zheng et al., 2017), metal organic frameworks (Sarkar et al., 2020a, 2020b; Xiao et al., 2018; Yang et al., 2017; Zhu et al., 2017), covalent organic frameworks (Wang et al., 2017) etc. Incorporation of these additives certainly improved the porosity in active separating layer by developing interspatial or intrinsic voids to channelize the water pathways. However, such incorporation often led to the formation of heterogeneous structure, reduction in mechanical strength, and solute selectivity due to development of grain boundary or undesired defects. Additionally, these steps augment further difficulty in scale up. Hence, preferably membrane materials should have high-interconnected free volume with narrow pore opening.

One of the notable class of microporous materials (pore size <2 nm), polymer with intrinsic microporosity (PIMs) and works on the principle of creating "*free volume*". PIMs have attracted significant attention as it targets to generate free volume by means of interconnected voids, and thus becomes a potential material in membrane-based separation process (McKeown and Budd, 2006; Budd et al., 2005; Swaidan et al., 2015; Wang et al., 2018). PIMs are structurally designed using highly rigid and contorted monomers (such as Spirobisindane), which polymerizes to deliver inefficient chain packing and generate interconnected voids of less than 2 nm (Ghanem et al., 2008; Alghunaimi et al., 2015; Carta et al., 2013; Gorgojo et al., 2014). The microporosity of PIMs has been efficiently used as a selective separating layer in organic solvent nanofiltration (OSN) (Gorgojo et al., 2014; Jimenez-Solomon et al., 2016), gas separations (Carta et al., 2013; Zhuang et al., 2014), and pervaporation applications (Adymkanov et al., 2008). In general, PIMs have been synthesized using the monophasic approach and the resulting polymers have shown microporosity, which have been transformed to thin films by solution-processing methods, like knife-casting or spin coating for membrane applications (Jimenez-Solomon et al., 2016).

Inspired by the concept of intrinsic microporosity, Livingstone and co-workers used the rigid and contorted monomer (Spirobisindane (TTSBI)) to introduce the new generation polyaryl-based microporous family of membranes. The thin-film composite (TFC) membrane of microporous polyaryl polymer was grown using interfacial polymerization technique onto porous support and further used for organic solvent nanofiltration (OSN) and gas separation (Jimenez-Solomon et al., 2016). The work opens up new avenue in the class of microporous polymers and next-generation membranes for molecular separation. The addition of such contorted monomer along with well-established IP-based nanofiltration membrane has reportedly provided enhanced microporosity (Jiang et al., 2019), with improved permeability (Around 2- to 3-fold increase (18 $Lm^{-2}h^{-1}bar^{-1}$) for Na_2SO_4 as compared to the pristine nanofiltration membrane. It also showed higher rejection of divalent salt (Na_2SO_4) as compared to monovalent salt (NaCl), along with the rejection of probe molecules with 300–400 MW, whereas the water permeance data for these membranes were lacking. Furthermore, the interfacial polymerization between TTSBI and isophthaloyl chloride generated the thin layer of highly microporous membrane supported on single-walled carbon nanotube, and showed the rejection of high molecular weight (MW ~ 700 $gmol^{-1}$) negatively charged dye molecules with high water permeance ~210 L $m^{-2}h^{-1}bar^{-1}$ (Lu et al., 2020). The family of membranes with characteristic features like incorporation of microporosity in the existing dense NF membrane and production of highly microporous new generation membranes showed improved performance to overcome permeance-selectivity trade-off with the low molecular high molecular weight (MW = 700–1,200 $gmol^{-1}$) probe/dye molecules. However, literature suggests the enhancement in permeance-selectivity trade-off in the range of 400–700 $gmol^{-1}$ molecular weight is challenging (Werber et al., 2016). Such trade-off in the range of 400–700 $gmol^{-1}$ molecular weight demands optimum free volume, thickness and cross-linking, and hydrophilicilty to achieve desire membrane for selective cut-off. So far, literature reports suggested that the use of contorted monomers (Jimenez-Solomon et al., 2016; Jiang et al., 2019; Lu et al., 2020) increases the microporosity by increasing the free volume. It also suggested that controlling the monomer diffusion in diffusion-driven IP leads to the thin and low cross-linked polymeric film. Overall, a combination of different parameters like free volume, hydrophilicity, and low cross-linking density certainly affects the pore aperture and pore size distribution and kinetics affects the thickness [Wang et al., 2021], if addressed will serve major gains in wastewater treatment.

In the present work, we developed thin separating layer of polyarylate nanofilm separating layer. The polyaryl nanofilm was characterized using microscopic analysis to know more about the surface morphology and thickness. The polyaryl nanofilm was supported onto ultrafiltration polyether (PES (Polyether sulfone)) support to form a composite membrane. The polyaryl nanofilm composite membrane is used as a selective layer for molecular weight cut-off and water permeance. The thin polymeric film is grown at interface using rigid, contorted TTSBI (Aqueous layer) and trimesoyl chloride (TMC) (Hexane layer). Optimization of the monomer concentration resulted into thin film (Approx. 15 nm). The present strategy provides thin separating layer of polyaryl (PAR) NF membrane that removes the molecules with the molecular weight above 450 g mol^{-1} high water permeance.

RESULTS

The polyaryl nanofilm at the solvent, non-solvent interphase was prepared using the well-reported interfacial polymerization technique (Please refer to supplemental information for details). The defect-free thin-film polyaryl membrane was synthesized by reacting the rigid, contorted spirobisindane monomer (TTSBI) with trimesoyl chloride (TMC) at the interface between two immiscible solutions (Figures 1 and S1) in presence of a base. The base abstracts the phenolic proton to form the sodium phenoxide, which is water-soluble, and diffuses it to the hexane layer to react with TMC. At the interface, thin polymeric film starts forming upon initiation of salt metathesis. The rigid and contorted shape of TTSBI monomer result into the polymer with inefficient packing of polymeric chains, and generate interconnected free volume. The thickness of polyaryl nanofilm at the interphase optimized with different concentration ratios of TTSBI and TMC, by evaluating their permeance efficiency for membrane separation (Discussed in separation section). The kinetics of the thin-film formation is controlled by optimizing monomer concentrations and reaction time to obtain a continuous defect-free thin film (Tables 1 and S1). The flexible polymeric chains offer the processability to prepare the tuneable thin films retaining the structural integrity and providing the controlled porosity due to the entangled polymeric chains arising from the contorted monomer.

The morphology and cross-sectional analysis of thin films are studied with the help of microscopic tools (Figures 2 and S2–S6). The cross-section of polyaryl nanofilms indicates the uniform thickness of the film,

Table 1. Pure water permeance at different concentration of TTSBI and TMC

TTSBI Concentration (mmol/L)	NaOH concentration (mmol/L)	TMC concentration in hexane (mmol/L)	Time (Interfacial polymerization)	Pure water permeance ($Lm^{-2}h^{-1}$ bar^{-1})[a]
0.02	8.33	37.7	1 min	32
0.2	8.33	37.7	1 min	110
2.0	8.33	37.7	1 min	37

[a]Pure water permeance was measured using cross-flow cell and details are provided in supporting information. The feed solution pumped with a flow rate of 1.1 L/min.

and after optimizing the concentration of monomers (1 mg, 0.0066% (w/v)) and reaction time (1 min), we could achieve a minimum continuous thickness of 14 $\pm$ 2 nm (Figures 2A–2C). Upon closer assessment, at a higher magnification with the help of transmission electron micrographs (TEM), it revealed the uniformity, stacking of various layers, folding, and further presence of chain-like structures in the thin film (Figures 2D–2G). The concentration and time to form the thin films optimized based on the pure water permeance as shown in Tables 1 and S1. The thin films picked on Si wafer, and showed uniform surface with linear and circular wrinkles in film (Figures 1 and S3–S6). The linear and circular wrinkles (crumpled morphology) are clearly observed on the polyaryl nanofilm, which does not collapse even after drying [Wang et al., 2021]. This development of crumpled morphology plays key role in enhancing active surface area for high permeance. Whereas after drying, the thin films remained continuous and devoid of any cracks on the surface. This all indicates the flexibility and elastic nature of the polymeric thin films. The ease in processability of thin films offered the advantage of preparing thin films with desired thickness and were recurrently grown and analyzed for their molecular cut-off potentials to define the nature of porosity in the thin films.

To study the structural features of the polymeric nanofilm, the bulk polyarylate polymer was prepared. The highly reactive acyl chloride groups of TMC and the hydroxyl group of TTSBI reacts to the formation of ester groups leading to the polyarylate polymer. The chemical composition of the polymer was determined by FTIR spetroscopy. As presented in FTIR spectra of PAR TTSBI polymer (Figure 3A), the peak at 1,750 cm^{-1} corresponds to the $C{=}O_{COOR}$ stretching frequency of ester groups indicating the formation of ester bonds in the polymer. Whereas, the peak at 3,450 cm^{-1} for O-HCOOH stretching, and 1,625 cm^{-1} for $C{=}O_{COOH}$ stretching of carboxylic acid, reflects the presence of free hanging carboxyl end group of the polymeric chain. The peak at 1,220 cm^{-1} indicates the $C\text{-}O_{COOR/COOH}$ stretching vibration supporting the presence of arylate polymer along with the carboxyl end groups. The characteristic peaks for the aromatic C=C stretching appear at 1,500 cm^{-1} and aromatic sp^2 C-H stretching and out of the plane bending vibration at 2,900 cm^{-1} and 675 cm^{-1} confirms the presence of aromatic rings in the polymer.

The pXRD analysis of the polyarylate polymer in Figure 3B showed broad peak ranging between 10° and 20° 2θ demonstrating the amorphous nature with short range order of PAR TTSBI polymer. The peak position is indicative of the microporosity in the polymer (Ali et al., 2020) with the lattice spacing value of 8.4 Å calculated using Scherrer's equation.

The thermal stability of the polyarylate polymer was studied by monitoring the weight loss due to the fractionation of volatile components upon constant heating with the help of TGA (Figure 3C). Thermal analysis of polyarylate polymer was studied in temperature range from 0°C to 800°C. The initial weight loss of 5% upto 150°C is due to the physically adsorbed water molecules. The weight loss of ~15% from 150°C to 300°C majorly corresponds to the loss of hydrogen-bonded water molecules participating in the network of intermolecular hydrogen bonding. The ~35% weight loss in the range of 300°C–500°C is due to the instability of ester bonds in polyarylate polymeric chains and their further fragmentation. Above 500°C temperature, the continuous and sharp weight loss of ~22% indicated the complete disintegration of the polymer.

The contact angle measurement used to derive surface hydrophilicity of the polyaryl nanofilm transferred on polyether sulfone (PES) ultrafiltration (UF) support. The measured water contact angle value of ~44° and ~47° (Figure 3D) for without hexane-water-washed and with hexane-water-washed membrane reveals that the polyaryl nanofilm is hydrophilic in nature. This could be due to the presence of surface carboxylate and

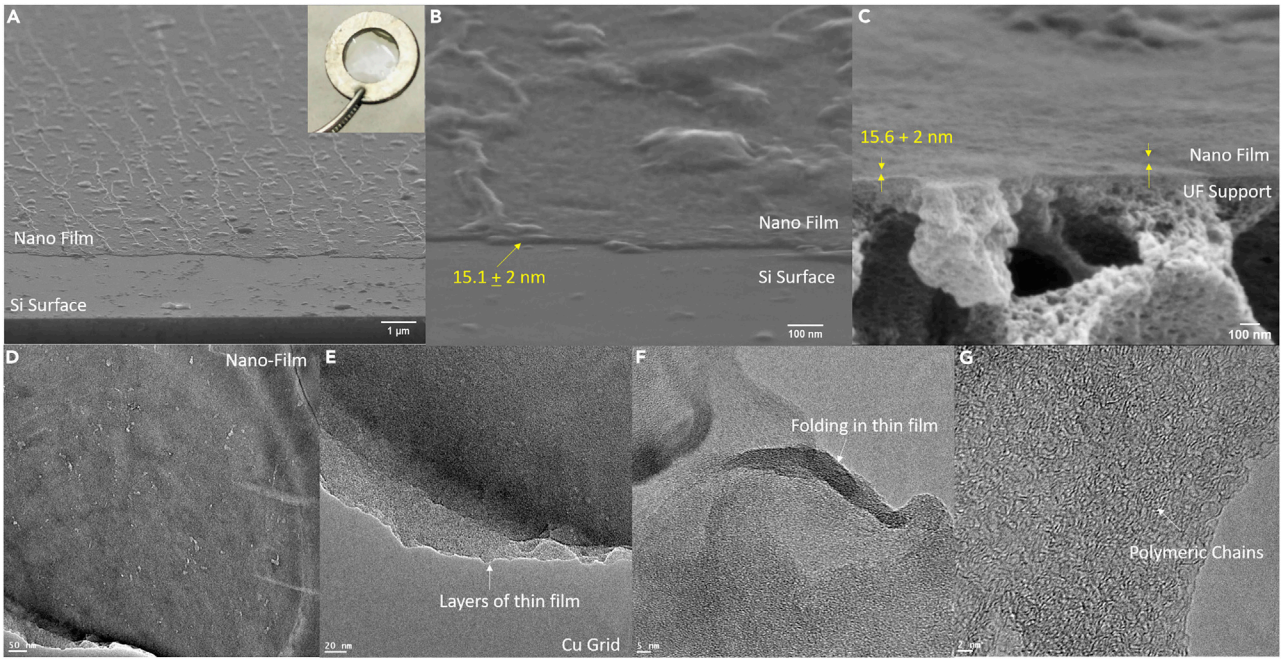

Figure 2. Morphological analysis to show the surface morphology as well as the cross-section of polyaryl nanofilms
(A–G) (A and B) FE-SEM images, (C) Nanofilm supported onto ultrafiltration support, (D–G) HRTEM images free-standing nanofilm.

residual hydroxyl group, which form hydrogen bonding with water molecule, reduces contact angle. Furthermore, surface charged distribution of the membrane was analyzed with zeta potential, using 1.0 mM KCl solution as background solution. The surface zeta potential measurement of the polyaryl nanofilms performed without hexa-water wash shows a negative (−11.85 mV) surface potential at pH 7. The presence of negative surface charge attributed to the presence of surface carboxylic group along with the residual phenoxy group. The surface negative charge is playing critical role in enhancing electrostatic repulsion between membrane surface and negatively charged dye or salt, and thus determining the selectivity of the polyaryl nanofilm.

The polyaryl nanofilms were used for nanofiltration applications in the form of thin-film composite membranes. Here, the thickness of separating top layer plays a decisive role in deciding the water permeability of membranes (Sarkar et al., 2020a, 2020b, 2021; Karan et al., 2015; Jiang et al., 2018; Tiwari et al., 2020); it has been observed that the water permeance is directly proportional to the thickness of nanofiltration membrane (Werber et al., 2016). Hence, the separating top-layer thickness of polyaryl membranes is fabricated by varying different concentration between TTSBI/TMC. A series of membranes were prepared by using different ratio of TTSBI:TMC, and it played a key role in controlling thickness of polyaryl nanofilms, which in turn showed a dramatic effect on membrane performance. Polyaryl nanofilms were tested against pure water permeance, and the results are shown in Table 1.

A high pure water permeance (PWP) of 100 $Lm^{-2}h^{-1}bar^{-1}$ was achieved with TTSBI: TMC (0.2 mmol/L: 37.7 mmol/L) for 1 min contact time (Table 1). Furthermore, increasing the monomer concentration (ten times), the PWP was found to decrease from 100 to 37 $Lm^{-2}h^{-1}bar^{-1}$ for TTSBI:TMC (2.0 mmol/L: 37.7 mmol/L) for 1 min contact time. The decrease in water permeance could be due to the formation of dense thick separating layer because of high concentration of TTSBI as compared to the polyaryl nanofilm developed at low TTSBI concentration. Interestingly, decrease in TTSBI concentration (ten times) TTSBI:TMC (0.02 mmol/L: 37.7 mmol/L) for 1 min contact time resulted into PWP 32 $Lm^{-2}h^{-1}bar^{-1}$. The unusual behavior of PWP is similar to the thin films of PIMs, where rigid contorted TTSBI reduces the solvent permeance below thickness of 100 nm (Gorgojo et al., 2014). Because at low concentration, even a rigid and contorted TTSBI monomer forms thin layers of polyaryl nanofilms, where polymer chains are structurally relaxed with diminished microporosity and decreased permeance. It is well established that polyamide nanofilms with crumpled (crease and wrinkles) structure generate enhanced active surface area and further

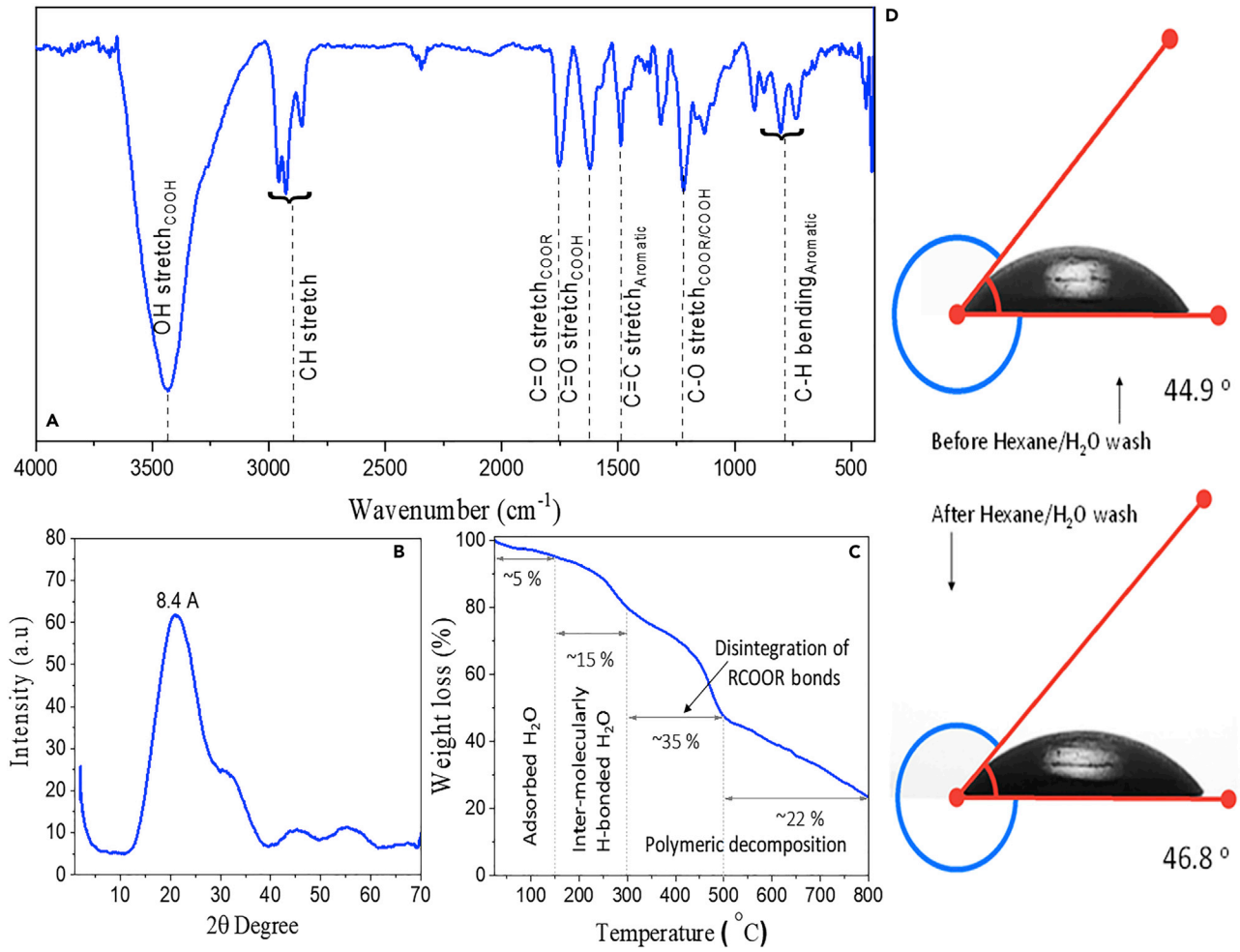

Figure 3. Characterization of polyarylate polymer

(A–D) (A) FTIR spectra, (B) pXRD pattern, (C) Thermal Analysis, (D) Contact angle measurement.

contribute to the high permeance of membranes (Sarkar et al., 2021; Karan et al., 2015). Polyaryl nanofilm formation using selected conditions [TTSBI:TMC (0.2 mmol/L: 37.7 mmol/L)] for 1 min contact time] showed high PWP. This could be due to the crumpled morphology of polyaryl nanofilm (Figures 2 and S3–S5) which remains intact at low operating pressure (1 bar).

The polyaryl nanofilm membrane was examined to evaluate separation performance in terms of permeance and rejection against various molecular markers, i.e. mono, di, and multivalent salts (NaCl, 2 gL^{-1}; Na_2SO_4, 2 gL^{-1}; and $K_3[Fe(CN)_6]$, 0.1 gL^{-1}), negatively charged dye molecules (7-Hydroxy-2-naphthalenesulfonic (HNSA), acid orange (AO), orange G (OG), acid fuchsin (AF), congo red (CR), and brilliant blue R (BBR); 0.1 gL^{-1} each).

Polyaryl nanofiltration results like rejection, permeance of molecular markers, and pure water permeance and their area are presented in Figure 4 (for further details please refer to supplemental information). High water permeability indicated the hydrophilic nature of the membrane. Hydrophilic nature of the membrane could be attributed to the free surface carboxylate group and residual hydroxyl groups. After formation of the polyaryl nanofilm, we did not perform hexane washing, rather allowed cross linking at high temperature in oven followed by immersion in cold water to attain hydrolysis.

Interestingly, the decrease in water permeance was observed (Figure 4B) in presence of salts and negatively charged markers, because of the limitation in mass transport and membrane fouling in the cell.

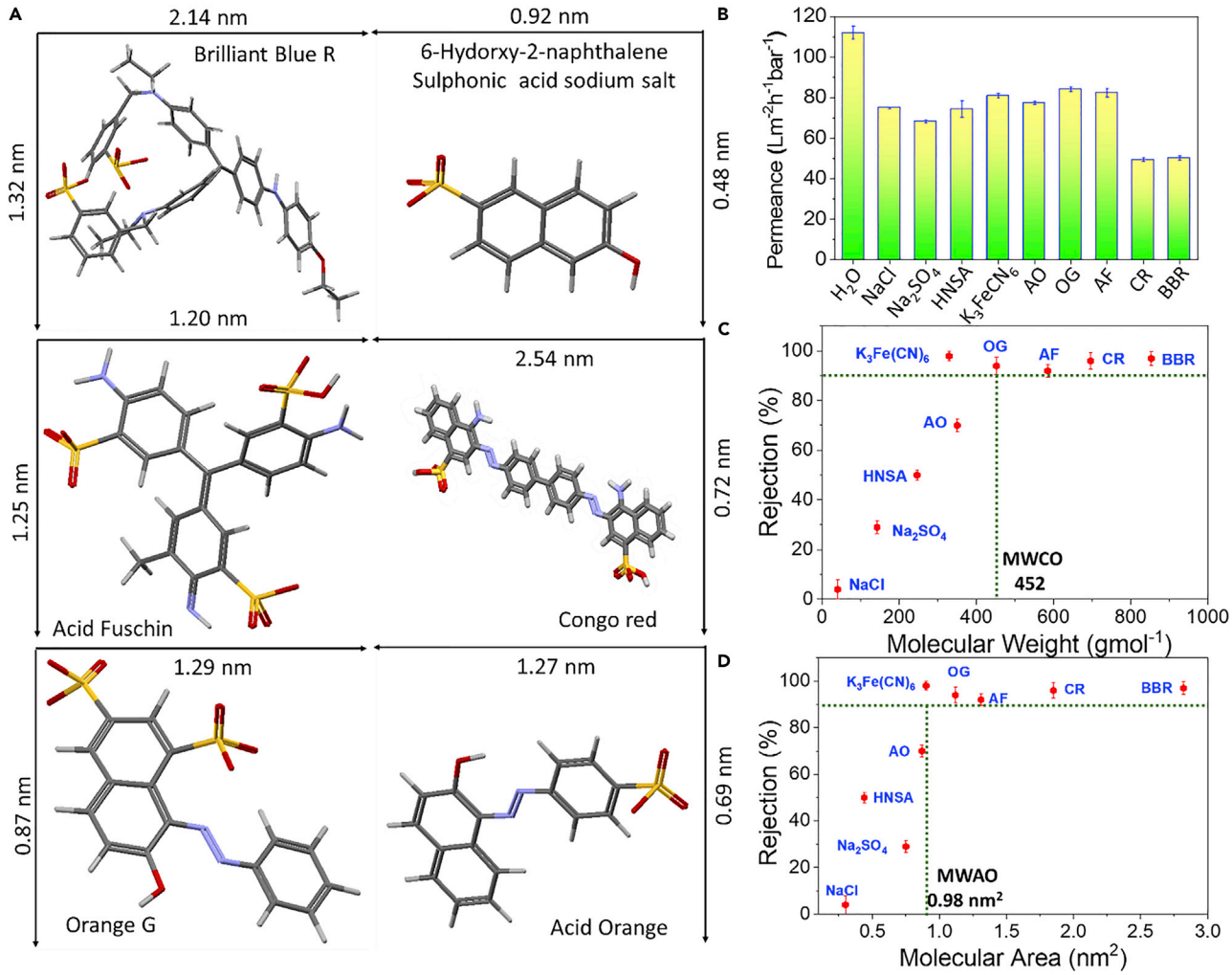

Figure 4. Nanofiltration performance with respect to various molecular markers

(A–D) (A) Dimensions of molecular markers, (B) Permeance of various molecular markers, (C) Molecular weight cut-off, and (D) Molecular area cut-off.

Polyaryl nanofilm composite membrane [TTSBI:TMC (1 mg (0.2 mmol/L: 37.7 mmol/L) for 1 min contact time] (Table 1) showed low rejection of ~4% for monovalent NaCl, ~29% for divalent Na_2SO_4, and high rejection of ~98% for multivalent $K_3[Fe(CN)_6]$ (Figures 4C and 4D). High water permeance >75 $Lm^{-2}h^{-1}bar^{-1}$ was achieved for mono and divalent salts whereas >80 $Lm^{-2}h^{-1}bar^{-1}$ permeance was achieved for multivalent salts. The rejection profile indicated that the polyaryl nanofilm maintained high rejection (>98%) for multivalent salt as compared to the divalent (29%) and monovalent salt (5%). The decrease in the water permeance in case of mono and divalent salts as compared to the multivalent salts is due to the mass transport. This is due to the relatively low osmotic pressure rise in case of multivalent salts with lower concentration (100 ppm). Whereas, higher concentration in the case of mono and divalent salts (2,000 ppm) generates concentration polarization, reduces water permeance. The present finding provides an excellent opportunity for the charge-based separation of salts while maintaining the high water recovery; it also showed improved balance between permeability and selectivity. Similarly, water flux of membrane under a dye solution is lower than that under pure water. This is because of greater osmotic pressure of dye solutions compared to pure water, as well as owing to the membrane pores being blocked by dye molecules. It is well established that physical property of solute and feed solution greatly osmotic pressure in filtration.

For better understanding, the polyaryl nanofilm for separation of negatively charged molecular probes with different molecular weight and molecular area was studied in term of their rejection and

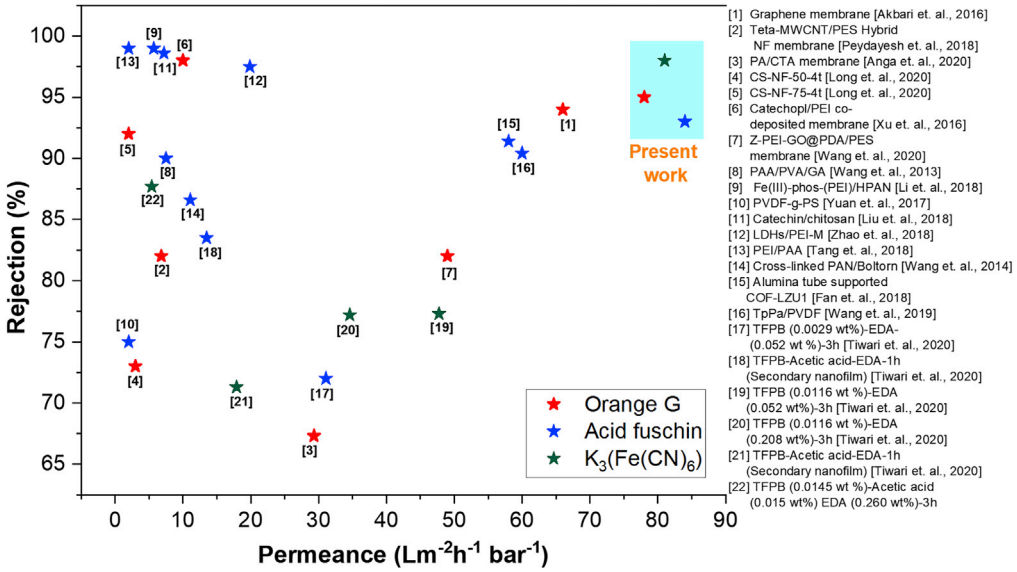

Figure 5. Comparison of the membrane performance of ultrathin (∼15 nm) polyaryl nanofilm with the present state-of-the-art membrane material using molecular marker (Dye molecule Orange G (MW = 452.38), Acid Fuchsin (MW = 585.53)) and multivalent salt (for e.g. $K_3[Fe[(CN)_6]$) (The details data are presented in Table S3)

permeability (Figures 4C and 4D). The polyaryl nanofilm presents high rejection for negatively charged molecular markers, e.g. brilliant blue R (>95%, BBR: 825.9 $gmol^{-1}$), congo red (>95%, CR: 696 $gmol^{-1}$), acid fuchsin (>90%, AF: 585 $gmol^{-1}$), orange G (>90%, OG: 452 $gmol^{-1}$), and acid orange (70%, AO: 350 $gmol^{-1}$) and moderate rejection for 6-hydroxy-2-naphthalene sulfonic acid sodium salt (50%, HNSA: 246 $gmol^{-1}$) (Figure S7). The UV-vis spectra for feed and permeate have been presented in Figure S7 for the molecular markers. Figure 4 represents the percentage of dye rejection, which indicates that the dye rejection is dependent on molecular weight (MW)/molecular area (MA). The Figure 4 also showed low rejection of smaller molecular weight marker (e.g HNSA) as compared to the other high molecular weight markers (For e.g. OG, AF, CR, and BBR). The dye molecules with the moderate range of MW cut-off (≥450 $gmole^{-1}$ (OG)) showed >90% rejection with the high water flux (>75 $Lm^{-2}h^{-1}$ bar^{-1}). The 452 MW cut-off dye has the MA of around 1.12 nm^2. Interestingly, > 95% rejection was observed in the case of $K_3[Fe(CN)_6]$, having MA of around 0.98 nm^2. The rejection data suggested that the polyaryl nanofilm follows the rejection mechanism of molecular sieving as well as electrostatic repulsion. Hence, polyaryl nanofilm showed preferred rejection toward high anionic charged salt (e.g $K_3[Fe(CN)_6]$; MA 0.98 nm^2), negatively charged molecular marker with molecular weight >450 $gmol^{-1}$ (OG with the MA 1.12 nm^2) (Table S2). This could be due to the presence of negative charge as well as pore aperture of <0.9 nm^2. To understand more about the pore aperture at molecular level, the polyaryl structure was optimized using Chem 3D software computational tool (Figure S8). The optimized structure suggested the four different types of pore having MA ranging from 0.3 to 0.8 nm^2. Thus, the polyaryl nanofilm rejects molecules using molecular sieving and electrostatic repulsion mechanism.

High water permeance through the polyaryl nanofilm was realized when the thickness was reduced to ∼15 nm. The fabricated ultrathin polyaryl nanofilm addresses the reduction of resistance associated with the thick composite membrane as separation layer. The development of a polyaryl nanofilm with the ultrathin separating layer in form of composite membrane can be used as high permeance membranes. In comparison with the crystalline composite membrane, thick separation layer may show crystal defect, and thus reduces the mechanical strength and thus limit their utility in many separation application.

Moreover, the synthesized polyaryl nanofilm membranes with surface morphology, hydrophilicity, and a thickness of ∼15 nm demonstrate high water permeance, and excellent molecular weight cut-off outperforms the most of the reported state-of-art membranes (Figure 5).

DISCUSSION

We report ultrathin (~15 nm) polyaryl nanofilm onto ultrafiltration support using an interfacial polymerization approach between TTSBI and TMC. The fabrication method resulted in high surface negative charge and hydrophilic character on the surface of polyaryl nanofilm. Microscopy study shows crumpled morphology throughout the surface devoid of cracks, and which does not collapse during testing. Ultrathin ~15 nm separating layer shows high water permeance (~110 $Lm^{-2}h^{-1}bar^{-1}$) and rejection of molecule with moderate MW (450 $gmole^{-1}$) with the water permeance of ~84 $Lm^{-2}h^{-1}bar^{-1}$. It is capable to remove multivalent salt ($K_3Fe(CN)_6$) as compared to the monovalent (~5%) and divalent salt (~28%) with the water permeance of ~81 $Lm^{-2}h^{-1}bar^{-1}$. The present work shows the utility of interfacial polymerization to produce thin microporous separating layer of composite membrane. This material has enormous opportunity to improve permselectivity in nanofiltration membrane for application window like waste-water treatment, molecular separation, and pharmaceutical sectors.

Limitations of the study

The high flux membranes have inherent limitation of pressure drop across the porous support where ultrathin polyaryl nanofilm layer of composite membrane resides. However, an appropriate suitable of support may even result into much higher liquid permeance without affecting the separation. Further understanding and development on the formation of the polyaryl nanofilms on highly porous ultrafiltration support are necessary to enhance superior membranes property for molecular separation.

STAR★METHODS

Detailed methods are provided in the online version of this paper and include the following:

- KEY RESOURCES TABLE
- RESOURCE AVAILABILITY
  - Lead contact
  - Materials availability
  - Data and code availability
- EXPERIMENTAL MODEL AND SUBJECT DETAILS
- METHOD DETAILS
  - Experimental procedure
  - Characterization techniques
- QUANTIFICATION AND STATISTICAL ANALYSIS

SUPPLEMENTAL INFORMATION

Supplemental information can be found online at https://doi.org/10.1016/j.isci.2022.104441.

ACKNOWLEDGMENTS

The authors are grateful to the Council of Scientific & Industrial Research, India for the financial support (AK, CSIR/JRF/31/028(0272)/2019-EMR-1; KP, CSIR-CSMCRI/MLP0043; and SK, CSIR-CSMCRI/MLP0045). MD is thankful to PIAS, Parul University, Vadodara, for allowing to complete his dissertation at CSIR-CSMCRI. The authors also acknowledge the analytical support from the CSIR-CSMCRI, Bhavnagar. A PRIS number (CSIR-CSMCRI-37/2022) has been assigned for this manuscript.

AUTHOR CONTRIBUTIONS

K.P. has conceptualized the project. A.K. carried out experiments, optimized thickness of membranes, and carried out detailed separation experiments using cross-flow cell. M.D. established preliminary preparation of thin films, bulk polymer, and separation experiments. P.D. performed long-run membrane experiments. P.D. and K.M. performed zeta potential and water contact angle. S.K. and K.P. supervised the project, performed data analysis, and wrote the manuscript.

DECLARATION OF INTERESTS

There are no competing interests.

Received: November 2, 2021
Revised: April 27, 2022
Accepted: May 16, 2022
Published: June 17, 2022

SUPPORTING CITATIONS

The following references appear in the supplemental information: Akbari et al., 2016; Anga et al., 2020; Fan et al., 2018; Li et al., 2018; Liu et al., 2018; Long et al., 2020; Peydayesh et al., 2018; Tang et al., 2013; Wang et al., 2013; Wang et al., 2014; Wang et al., 2019; Wang et al., 2020; Xu et al., 2016; Yuan et al., 2017; Zhao et al., 2018.

REFERENCES

Adymkanov, S.V., Yampol'Skii, Y.P., Polyakov, A.M., Budd, P.M., Reynolds, K.J., Mckeown, N.B., and Msayib, K.J. (2008). Pervaporation of alcohols through highly permeable PIM-1 polymer films. Polym. Sci. *50*, 444–450. https://doi.org/10.1134/s0965545x08040135.

Akbari, A., Sheath, P., Martin, S.T., Shinde, D.B., Shaibani, M., Banerjee, P.C., Tkacz, R., Bhattacharyya, D., and Majumder, M. (2016). Large-area graphene-based nanofiltration membranes by shear alignment of discotic nematic liquid crystals of graphene oxide. Nat. Commun. *7*, 10891. https://doi.org/10.1038/ncomms10891.

Alghunaimi, F., Ghanem, B., Alaslai, N., Swaidan, R., Litwiller, E., and Pinnau, I. (2015). Gas permeation and physical aging properties of triptycene diamine-based microporous polimides. J. Membr. Sci. *490*, 321–327. https://doi.org/10.1016/j.memsci.2015.05.010.

Ali, Z., Ghanem, B.S., Wang, Y., Pacheco, F., Ogieglo, W., Vovusha, H., Genduso, G., Schwingenschlögl, U., Han, Y., and Pinnau, I. (2020). Finely tuned submicroporous thin-film molecular sieve membranes for highly efficient fluid separations. Adv. Mater. *32*, 2001132. https://doi.org/10.1002/adma.202001132.

Anga, M.B.M.Y., Luo, Z.-Y., Marquez, J.A.D., Tsai, H.-A., Huang, S.-H., Hung, W.-S., Hu, C.-C., Lee, K.-R., and Lai, J.-Y. (2020). Merits of using cellulose triacetate as a substrate in producing thin-film composite nanofiltration polyamide membranes with ultra-high performance. J. Taiwan Inst. Chem. Eng. *112*, 251–258. https://doi.org/10.1016/j.jtice.2020.06.008.

Budd, P.M., McKeown, N.B., and Fritsch, D. (2005). Free volume and intrinsic microporosity in polymers. J. Mater. Chem. *15*, 1977–1986. https://doi.org/10.1039/b417402j.

Carta, M., Malpass-Evans, R., Croad, M., Rogan, Y., Jansen, J.C., Bernardo, P., Bazzarelli, F., and McKeown, N.B. (2013). An efficient polymer molecular sieve for membrane gas separation. Science *339*, 303–307. https://doi.org/10.1126/science.1228032.

Cheng, X., Ding, S., Guo, J., Zhang, C., Guo, Z., and Shao, L. (2017). In-situ interfacial formation of TiO_2/polypyrrole selective layer for improving the separation efficiency towards molecular separation. J. Membr. Sci. *536*, 19–27. https://doi.org/10.1016/j.memsci.2017.04.057.

Elimelech, M., and Phillip, W.A. (2011). The future of seawater desalination: energy, technology, and the environment. Science *333*, 712–717. https://doi.org/10.1126/science.1200488.

Fan, H., Gu, J., Meng, H., Knebel, A., and Caro, J. (2018). High-flux membranes based on the covalent organic FrameworkCOF-LZU1 for SelectiveDye separation by nanofiltration. Angew. Chem. Int. Ed. *57*, 4083–4087. https://doi.org/10.1002/anie.201712816.

Fane, A.G., Wang, R., and Hu, M.X. (2015). Synthetic membranes for water purification: status and future. Angew. Chem. Int. Ed. *54*, 3368–3386. https://doi.org/10.1002/anie.201409783.

Geise, H.B., Park, H.B., Sagle, A.C., Freeman, B.D., and McGrath, J.E. (2011). Water permeability and water/salt selectivity tradeoff in polymers for desalination. J. Membr. Sci. *369*, 130–138. https://doi.org/10.1016/j.memsci.2010.11.054.

Ghanem, B.S., McKeown, N.B., Budd, P.M., Selbie, J.D., and Fritsch, D. (2008). High-performance membranes from polyimides with intrinsic microporosity. Adv. Mater. *20*, 2766–2771. https://doi.org/10.1002/adma.200702400.

Gorgojo, P., Karan, S., Wong, H.C., Jimenez-Solomon, M.F., Cabral, J.T., and Livingston, A.G. (2014). Ultrathin polymer films with intrinsic microporosity: anomalous solvent permeation and high flux membranes. Adv. Funct. Mater. *24*, 4729–4737. https://doi.org/10.1002/adfm.201400400.

Guiver, M.D., and Lee, Y.M. (2013). Polymer rigidity improves microporous membranes. Science *339*, 284–285. https://doi.org/10.1126/science.1232714.

Hu, R., He, Y., Zhang, C., Zhang, R., Li, J., and Zhu, H. (2017). Graphene oxide-embedded polyamide nanofiltration membranes for selective ion separation. J. Mater. Chem. *5*, 25632–25640. https://doi.org/10.1039/c7ta08635k.

Jiang, C., Tian, L., Hou, Y., and Niu, Q.J. (2019). Nanofiltration membranes with enhanced microporosity and inner-pore interconnectivity for water treatment: excellent balance between permeability and selectivity. J. Membr. Sci. *586*, 192–201. https://doi.org/10.1016/j.memsci.2019.05.075.

Jiang, Z., Karan, S., and Livingston, A.G. (2018). Water transport through ultrathin polyamide nanofilms used for reverse osmosis. Adv. Mater. *30*, 1705973. https://doi.org/10.1002/adma.201705973.

Jimenez-Solomon, M.F., Song, Q., Jelfs, K.E., Munoz-Ibanez, M., and Livingston, A.G. (2016). Polymer nanofilms with enhanced microporosity by interfacial polymerization. Nat. Mater. *15*, 760–767. https://doi.org/10.1038/nmat4638.

Karan, S., Jiang, Z., and Livingston, A.G. (2015). Sub-10nmpolyamide nanofilms with ultrafast solvent transport for molecular separation. Science *348*, 1347–1351. https://doi.org/10.1126/science.aaa5058.

Li, P., Wang, Z., Yang, L., Zhao, S., Song, P., and Khan, B. (2018). A novel loose-NF membrane based on the phosphorylation and cross-linking of polyethyleneimine layer on porous PAN UF membranes. J. Membr. Sci. *555*, 56–68. https://doi.org/10.1016/j.memsci.2018.03.018.

Liang, B., Wang, H., Shi, X., Shen, B., He, X., Ghazi, Z.A., Khan, N.A., Sin, H., Khattak, A.M., Li, L., and Tang, Z. (2018). Microporous membranes comprising conjugated polymers with rigid backbones enable ultrafast organic-solvent nanofiltration. Nat. Chem. *10*, 961–967. https://doi.org/10.1038/s41557-018-0093-9.

Liu, S., Wang, Z., and Song, P. (2018). Free radical graft copolymerization strategy to prepare catechin-modified chitosan loose nanofiltration (NF) membrane for dye desalination. ACS Sustain. Chem. Eng. *6*, 4253–4263. https://doi.org/10.1021/acssuschemeng.7b04699.

Liu, T.Y., Liu, Z.H., Zhang, R.X., Wang, Y., Bruggen, B.V.d., and Wang, X.L. (2015). Fabrication of a thin film nanocomposite hollow fiber nanofiltration membrane for wastewater treatment. J. Membr. Sci. *488*, 92–102. https://doi.org/10.1016/j.memsci.2015.04.020.

Long, Q., Zhang, Z., Qi, G., Wang, Z., Chen, Y., and Liu, Z.-Q. (2020). Fabrication of chitosan nanofiltration membranes by the film casting strategy for effective removal of dyes/salts in textile wastewater. ACS Sustain. Chem. Eng. *8*, 2512–2522. https://doi.org/10.1021/acssuschemeng.9b07026.

Lu, Y., Fang, W., Kong, J., Zhang, F., Wang, Z., Teng, X., Zhu, Y., and Jin, J. (2020). A microporous polymer ultrathin membrane for the highly efficient removal of dyes from acidic saline solutions. J. Membr. Sci. *603*, 118027. https://doi.org/10.1016/j.memsci.2020.118027.

McKeown, N.B., and Budd, P.M. (2006). Polymers of intrinsic microporosity (PIMs): organic materials for membrane separations, heterogeneous catalysis and hydrogen storage. Chem. Soc. Rev. *37*, 675–683. https://doi.org/10.1002/chin.200645246.

Peydayesh, M., Mohammadi, T., and Bakhtiari, O. (2018). Effective treatment of dye wastewater via positively charged TETA-MWCNT/PES hybrid nanofiltration membranes. J. Sep. Pur. *194*, 488–502. https://doi.org/10.1016/j.seppur.2017.11.070.

Rezakazemi, M., Khajeh, A., and Mohammad Mesbah, M. (2018). Membrane filtration of wastewater from gas and oil production. Environ. Chem. Lett. *16*, 367–388. https://doi.org/10.1007/s10311-017-0693-4.

Sarkar, P., Modak, S., and Karan, S. (2020a). Effect of porous and nonporous nanostructures on the permeance of positively charged nanofilm composite membranes. Adv. Mater. Interfac. *7*, 2000251. https://doi.org/10.1002/admi.202000251.

Sarkar, P., Modak, S., and Karan, S. (2020b). Ultraselective and highly permeable polyamide nanofilms for ionic and molecular nanofiltration. Adv. Funct. Mater. *31*, 2007054. https://doi.org/10.1002/adfm.202007054.

Sarkar, P., Modak, S., Ray, S., Adupa, V., Reddy, K.A., and Karan, S. (2021). Fast water transport through sub-5 nm polyamide nanofilms: the new upper-bound of the permeance–selectivity trade-off in nanofiltration. J. Math. Chem. A *9*, 20714–20724. https://doi.org/10.1039/d1ta04763a.

Shen, J.N., Yu, C.c., Ruan, H.m., Gao, C.j., and Van der Bruggen, B. (2013). Preparation andcha racterization of thin-film nanocomposite membranes embedded with poly(methyl methacrylate) hydrophobic modified multiwalled carbon nanotubes by interfacial polymerization. J. Membr. Sci. *442*, 18–26. https://doi.org/10.1016/j.memsci.2013.04.018.

Sholl, D.S., and Lively, R.P. (2016). Seven chemical separations to change the world. Nature *532*, 435–437. https://doi.org/10.1038/532435a.

Soroko, I., and Livingston, A. (2009). Impact of TiO_2 nanoparticles on morphology and performance of crosslinked polyimide organic solvent nanofiltration (OSN) membranes. J. Membr. Sci. *343*, 189–198. https://doi.org/10.1016/j.memsci.2009.07.026.

Swaidan, R., Ghanem, B., and Pinnau, I. (2015). Fine-tuned intrinsically ultramicroporous polymers redefine the permeability/selectivity upper bounds of membrane-based air and hydrogen separations. ACS Macro Lett. *4*, 947–951. https://doi.org/10.1021/acsmacrolett.5b00512.

Tan, Z., Chen, S., Peng, X., Zhang, L., and Gao, C. (2018). Polyamide membranes with nanoscale Turing structures for water purification. Science *360*, 518–521. https://doi.org/10.1126/science.aar6308.

Tang, H., Ji, S., Gong, L., Guo, H., and Zhang, G. (2013). Tubular ceramic-based multilayer separation membranes using spray layer-by-layer assembly. Polym. Chem. *4*, 5621–5628. https://doi.org/10.1039/c3py00617d.

Tavangar, T., Karimi, M., Rezakazemi, M., Reddy, K.R., and Aminabhavi, T.M. (2020). Textile waste, dyes/inorganic salts separation of cerium oxide-loaded loose nanofiltration polyethersulfone membranes. Chem. Eng. J. *385*, 123787. https://doi.org/10.1016/j.cej.2019.123787.

Tiwari, K., Sarkar, P., Modak, S., Singh, H., Pramanik, S.K., Karan, S., and Das, A. (2020). Large area self-assembled ultrathin polyimine nanofilms formed at the liquid–liquid interface used for molecular separation. Adv. Mater. *32*, 1905621. https://doi.org/10.1002/adma.201905621.

Wang, L., Ji, S., Wang, N., Zhang, R., Zhang, G., and Li, J.-R. (2014). One-step self-assembly fabrication of amphiphilic hyperbranched polymer composite membrane from aqueous emulsion for dye desalination. J. Membr. Sci. *452*, 143–151. https://doi.org/10.1016/j.memsci.2013.10.034.

Wang, C., Feng, Y., Chen, J., Bai, X., Ren, L., Wang, C., Huang, K., and Wu, H. (2020). Nanofiltration membrane based on graphene oxide crosslinked with zwitterion-functionalized polydopamine for improved performances. J. Taiwan Inst. Chem. Eng. *110*, 153–162. https://doi.org/10.1016/j.jtice.2020.03.009.

Wang, C., Li, Z., Chen, J., Li, Z., Yin, Y., Cao, L., Zhong, Y., and Wu, H. (2017). Covalent organic framework modified polyamide nanofiltration membrane with enhanced performance for desalination. J. Membr. Sci. *523*, 273–281. https://doi.org/10.1016/j.memsci.2016.09.055.

Wang, L., Wang, N., Zhang, G., and Ji, S. (2013). Covalent crosslinked assembly of tubular ceramic-based multilayer nanofiltration membranes for dye desalination. AlChE J *59*, 3834–3842. https://doi.org/10.1002/aic.14093.

Wang, R., Shi, X., Zhang, Z., Xiao, A., Sun, S.-P., Cui, Z., and Wang, Y. (2019). Unidirectional diffusion synthesis of covalent organic frameworks (COFs) on polymeric substrates for dye separation. J. Memb. Sci. *586*, 274–280. https://doi.org/10.1016/j.memsci.2019.05.082.

Wang, Y., Ma, X., Ghanem, B.S., Alghunaimi, F., Pinnau, I., and Han, Y. (2018). Polymers of intrinsic microporosity for energy-intensive membrane-based gas separations. Mater. Today Nano *3*, 69–95. https://doi.org/10.1016/j.mtnano.2018.11.003.

Wang, Z., Liang, S., Kang, Y., Zhao, W., Xia, Y., Yang, J., Wang, H., and Zhang, X. (2021). Manipulating interfacial polymerization for polymeric nanofilms of composite separation membranes. Prog. Polym. Sci. *122*, 101450. https://doi.org/10.1016/j.progpolymsci.2021.101450.

Werber, J.R., Osuji, C.O., and Elimelech, M. (2016). Materials for next-generation desalination and water purification membranes. Nat. Rev. Mater. *1*, 16018–16115. https://doi.org/10.1038/natrevmats.2016.18.

Xiao, F., Wang, B., Hu, X., Nair, S., and Chen, Y. (2018). Thin film nanocomposite membrane containing zeolitic imidazolate framework-8 via interfacial polymerization for highly permeable nanofiltration. J. Taiwan Inst. Chem. Eng. *83*, 159–167. https://doi.org/10.1016/j.jtice.2017.11.033.

Xu, Y.-C., Wang, Z.-X., Cheng, X.-Q., Xiao, Y.C., and Shao, L. (2016). Positively charged nanofiltration membranes via economically mussel-substance-simulated co-deposition for textile wastewater treatment. Chem. Eng. J. *303*, 555–564. https://doi.org/10.1016/j.cej.2016.06.024.

Yang, L., Wang, Z., and Zhang, J. (2017). Highly permeable zeolite imidazolate framework composite membranes fabricated via a chelation-assisted interfacial reaction. J. Mater. Chem. *5*, 15342–15355. https://doi.org/10.1039/c7ta03244g.

Yuan, F., Yang, Y., Wang, R., and Chen, D. (2017). Poly(vinylidene fluoride) grafted polystyrene (PVDF-g-PS) membrane based on in situ polymerization for solvent resistant nanofiltration. RSC Adv. *7*, 33201–33207. https://doi.org/10.1039/c7ra03998k.

Zhai, Z., Jiang, C., Zhao, N., Dong, W., Lan, H., Wang, M., and Niu, Q.J. (2018). Fabrication of advanced nanofiltration membranes with nanostrand hybrid morphology mediated by ultrafast Noria–polyethyleneimine codeposition. J. Mater. Chem. *6*, 21207–21215. https://doi.org/10.1039/c8ta08273a.

Zhang, F., Fan, J.b., and Wang, S. (2020). Interfacial polymerization: from chemistry to functional materials. Angew. Chem. Int. Ed. *59*, 21840–21856. https://doi.org/10.1002/anie.201916473.

Zhang, H.L., Gao, Y.B., and Gai, J.G. (2018). Guanidinium-functionalized nanofiltration membranes integrating anti-fouling and antimicrobial effects. J. Mater. Chem. *6*, 6442–6454. https://doi.org/10.1039/c8ta00342d.

Zhao, S., Zhu, H., Wang, Z., Song, P., Ban, M., and Song, X. (2018). A loose hybrid nanofiltration membrane fabricated via chelating-assisted in-situ growth of Co/Ni LDHs for dye wastewater treatment. Chem. Eng. J. *353*, 460–471. https://doi.org/10.1016/j.cej.2018.07.081.

Zheng, J., Li, M., Yu, K., Hu, J., Zhang, X., and Wang, L. (2017). Sulfonated multiwall carbon nanotubes assisted thin-film nanocomposite membrane with enhanced water flux and anti-fouling property. J. Membr. Sci. *524*, 344–353. https://doi.org/10.1016/j.memsci.2016.11.032.

Zhu, J., Qin, L., Uliana, A., Hou, J., Wang, J., Zhang, Y., Li, X., Yuan, S., Li, J., Tian, M., et al. (2017). Elevated performance of thin film nanocomposite membranes enabled by modified hydrophilic mofs for nanofiltration. ACS Appl. Mater. Interfac. *9*, 1975–1986. https://doi.org/10.1021/acsami.6b14412.

Zhuang, Y., Seong, J.G., Do, Y.S., Jo, H.J., Cui, Z., Lee, J., Lee, Y.M., and Guiver, M.D. (2014). Intrinsically microporous soluble polyimides incorporating trögers base for membrane gas separation. Macromolecules *47*, 3254–3262. https://doi.org/10.1021/ma5007073.

STAR★METHODS

KEY RESOURCES TABLE

REAGENT or RESOURCE	SOURCE	IDENTIFIER
Chemicals, solvents, salts, and dyes		
3,3,3′,3′-Tetramethyl-1,1′-spirobiindane-5,5′,6,6′-tetraol, 96.0%	Sigma-Aldrich (India)	CAS: 77-08-7
Trimesolyl chloride (1,3,5-Benzenetricarbonyltrichloride), 98.0%	Sigma-Aldrich (India)	CAS: 4422-95-1
Acid orange	TCI Chemicals (India)	CAS: 633-96-5
Orange G	TCI Chemicals (India)	CAS: 1936-15-8
Brilliant blue R	TCI Chemicals (India)	CAS: 6104-59-2
Congo red		
NaCl (99.9%)	Sisco Research Laboratories Pvt. Ltd., India	CAS: 7647-14-5
NaOH (98%)	Sisco Research Laboratories Pvt. Ltd., India	CAS: 1310-73-2
Na_2SO_4 (99.5%)	Sisco Research Laboratories Pvt. Ltd., India	CAS: 7757-82-6
Potassium Ferricyanide extrapure (98%)	Sisco Research Laboratories Pvt. Ltd., India	CAS:13746-66-2
n-Hexane pure (99%)	Sisco Research Laboratories Pvt. Ltd., India	CAS: 110-54-3
Acetone extrapure (99%)	Sisco Research Laboratories Pvt. Ltd., India	CAS: 67-64-1
Isopropanol, AR	MERCK Millipore, India	CAS: 67-63-0
Methanol, AR	MERCK Millipore, India	CAS: 67-56-1
Acetonitrile, AR	MERCK Millipore, India	CAS: 75-05-8
Dimethylformamide; 99% EMPLURA®	MERCK Millipore, India	CAS: 68-12-2
Polymers, membranes and substrates		
Polyethersulfone (PES) powder	Solvay, India	NA
Nonwoven polyester fabric	Nordlys-TS100, Polymer Group Inc., France	NA
N-type <100 > silicon wafer	University wafer, Boston, USA	https://universitywafer.com/

RESOURCE AVAILABILITY

Lead contact

Further information and requests for resources and reagents should be directed to and will be fulfilled by the lead contact, Ketan Patel (ketanpatel@csmcri.res.in).

Materials availability

This study did not generate new unique reagents.

Data and code availability

- Data: All data reported in this paper will be shared by the lead contact upon request.
- Code: This paper does not report the original code.
- Any additional information required to reanalyze the data reported in this paper is available from the lead contact upon request.

EXPERIMENTAL MODEL AND SUBJECT DETAILS

The study do not report any experimental models.

METHOD DETAILS

Experimental procedure

Preparation of polyther sulphone (PES) support membranes via phase inversion

The PES membranes were prepared according to the reported procedure (Sarkar et al., 2020a, 2020b) by phase inversion technique. PES polymer was dried in oven at 70°C for two hours, and then dried PES was

dissolved in DMF at 70°C with constant stirring in an airtight glass bottle to make 13% w/v solution. Then polymer solution was cooled down at 25°C. The membrane sheet was continuously casted on the nonwoven fabric at a speed of 4–7 m/min using semi-continuous casting machine. During this process, a polymer solution was casted on nonwoven fabric by diffusion of DMF by Water as a non-solvent with thickness of 130–150 micrometre at 25°C. After casting, the membranes were washed with DI water and kept in DI water for 2 days before the final storage at 10°C in isopropanol and water mixture (1:1) w/w%.

Synthesis of free standing polyaryl nanofilm

The free standing polyaryl nanofilms were synthesized using condensation polymerization at the interphase. Contorted monomer (5,5′,6,6′-tetrahydroxy-3,3,3′,3′- tetra methyl spirobisindane (TTSBI)) was used for interfacial polymerization, and dissolved in a diluted sodium hydroxide aqueous solution, with molar ratio of 4:1 (NaOH to TTSBI) with varied concentrations of TTSBI (0.1 mg in 15 mL of NaOH solution, 1 mg in 15 mL of NaOH solution, 10 mg in 15 mL of NaOH solution). A solution of 0.1% (w/v) TMC in hexane slowly added to the aqueous solution, and allowed to react for 1 min. The ratio between the concentrations of the two immiscible phases was kept 10:1, (concentration of the hexane phase should be 10 times lower than the aqueous phase). Afterwards, the resulting polyaryl nanofilms immediately withdrawn from the interface with a clean glass substrate, washed with clean distilled water. Thick free-standing film of polyaryl polymers were achieved by increasing the reaction time. Free-standing polyaryl nanofilm was clearly visible with all the different concentration at the interphase.

Synthesis of polyaryl nanofilm composite membranes

The nanofilm composite membranes for water based molecular sieving were prepared by interfacial polymerization directly on conditioned cross-linked Polyether sulphone (PES) supports. The PES Support was then thoroughly washed with water to remove the excess IPA (when it was stored in IPA). A Boat (active area 95 cm^2) was made from the support, by folding the edges of a support to make a rectangular boat, wash it thoroughly before use. Interfacial polymerization to form polyarylate Nanofilms was performed by exposing the surface of the PES support boat to an aqueous basic solution containing the sodium phenoxide ions, and TTSBI (0.1 mg in 15 mL of NaOH solution, 1 mg in 15 mL of NaOH solution, 10 mg in 15 mL of NaOH solution) for 2 min. The phenoxide-loaded support membranes were gently decanted and the support was pressed with a rubber roller to remove excess solution. The membranes were then exposed to TMC in hexane (0.1% w/v) for 1 min. The hexane solution was decanted and the resulting membranes were dried in air (2 min), and then in a Hot air oven at 90°C for 10 min to complete cross-linking. The resulting membranes were immediately stored in distilled water at 4°C.

Synthesis of polyarylate polymer

The bulk polyarylate polymer was prepared for characterization of its structural features. To obtain the bulk polyarylate polymer NaOH was first dissolved in distilled water, to which the monomer was added (4:1 Molar Ratio for TTSBI (1 gm), which resulted in the formation of phenoxide ion. To the aqueous phase of TTSBI, the solution of 0.1 wt% TMC in hexane was added, which resulted in the formation of a film at the interface. The reaction mixture was kept in vigorous stirring for 10 min, which resulted in the formation of polyarylate polymer. The resulting polyarylate polymer was washed with water followed by hexane and dried at 120°C for 12 hours. The solid amorphous polymers were than collected for further analysis.

Performance evaluation of the polyaryl nanofilm composite membrane

The nanofiltration performance of the polyaryl nanofilm composite membranes was tested in a cross-flow filtration setup. Feed solution (≈1 L) was pumped from a feed tank by using a diaphragm pump into the membrane cell. The effective area of the membranes used in the cell was 14.5 cm^2. Membranes were pre-compacted for at least 4 h under 2 bar pressure by using pure water to reach the steady-state condition. Membrane permeances was calculated using the following equation:

$$P = V/A \cdot t \cdot \Delta p \qquad \text{(Equation S1)}$$

where V is the volume of the permeate in Liters, t (h) is the collection time, A (m^2) is the effective area of the membrane used, Δp (bar) is the transmembrane pressure.

Membrane permeances were continuously monitored and the feed and permeate solutions were collected for the analysis. The separation performance of the membranes was analyzed using different salts and dyes

added in the feed solution. The concentration of NaCl and Na_2SO_4 salt was 2 $g.L^{-1}$ (2000 ppm) and for $K_3[Fe(CN)_6]$ was 0.1 $g.L^{-1}$ (100 ppm). The concentration of 7-Hydroxy-2-naphthalenesulfonic (HNSA), acid orange (AO), orange G (OG), acid fuchsin (AF), congo red (CR), and brilliant blue R (BBR) in the feed was 0.1 $g.L^{-1}$(100 ppm). The concentration of salts and dyes in the permeate and the feed was measured by an electrical conductivity meter and by the UV-visible absorbance values respectively. The rejection (R) of membranes was calculated as a percentage according to the following equation:

$$(\%) = \left(1 - C_p / C_f\right) \times 100 \qquad \text{(Equation S2)}$$

where, C_p (in $g.L^{-1}$) and C_f (in $g.L^{-1}$) are the concentrations of solutes in the permeate and the feed, respectively. At least four membrane coupons were tested to get an average value and standard deviation.

Characterization techniques

The freestanding nanofilms and nanofilm composite membranes were analysed for the surface and cross-sectional morphology using the scanning electron microscope (SEM; JEOL, JSM 7100F). The samples were prepared by picking the freestanding interfacial polyaryl nanofilm from the liquid-liquid interface at different time intervals onto silicon wafer and vaccum dried, followed by thin layer gold coating for FESEM. A small piece was fractured-cut from the support and placed vertically in the SEM sample stub to determine the thickness of the polyaryl nanofilm. Carbon tape adhesive was used to fix the samples in the stab as well as to avoid sample charging during SEM imaging.

The surface morphology of the polyaryl nanofilms was also studied using transmission electron microscopy TEM (JEOL, JEM-2100) equipped with LaB6 filament, operating at an accelerating voltage of 120 keV. The samples were prepared by picking thin film from the liquid-liquid interface at different time intervals onto the lacey coated copper grid and vaccum dried. An optical microscope (Leica DM-750 Leica Microsystems), was used to visualize the films formation by placing the polyaryl nanofilms on a glass slide, and visualising it with the lens having a white light source from the beneath.

The water contact angle of the composite membrane was measured with a drop shape analyser using macro lens modes. Nanofilm composite membranes were freshly prepared on PES support via interfacial polymerization. Membranes were washed with water by immersing them for 10 min in the water bath and dried in a hot air oven at 50 ($\pm$1) °C. Samples were prepared by fixing them on glass micro-slides using both-sided adhesive tape. The contact angle was measured in triplicate to estimate the average value of the contact angle.

The surface charge of the polyaryl nanofilm was evaluated in a ZetaCad streaming current & zeta potential meter, CAD Instruments, France. The composite membranes made on PES (Polyethyer sulfone) support were wetted in water for a few hours and placed in the dedicated flat sheet test cell. The steady-state zeta potential values were recorded with a 1 mM KCl electrolyte solution. The experiments were performed in triplicate to obtain the mean value and the standard deviation of the measurements. Two pieces of membranes with a dimension of 3 × 5 cm^2 were cut and kept in the KCl solution overnight before use. Zeta potential values were obtained at pH 7 using a 1 M KCl solution.

An electrical conductivity meter (Eutech PC2700) was used to measure the conductivity of feed and permeate samples and to calculate the salt rejection of the membranes. Ground state optical absorption of the aqueous solution was measured in a quartz cell (light path 10 mm) on an UV-vis spectrophotometer (UV-2700, Shimadzu) equipped with a PTC- 348WI temperature controller. The concentration of all the molecular markers was calculated by measuring the absorbance of feed (F) and permeate (P). FTIR spectra were collected over the frequency range 4,000–400 cm^{-1} by the KBr pellet method using an IR spectrometer (Perkin Elmer, Spectrum GX) with 4 cm^{-1} resolution at room temperature. For the pXRD study, Cu-Kα radiation was used and the data recorded over a 2θ range of 5–80°. Thermal analyses was performed with a Mettler Toledo and Netzsch Thermogravimetric analyzer (TGA) Q500 with temperature range of 25°–800°C.

QUANTIFICATION AND STATISTICAL ANALYSIS

We report the average values of water permeance, salt, and molecular marker rejections, and standard deviations of the results based on the measurements of at least four sets of membrane coupons.